Letters

Virtual Synchronous Machine integration on a Commercial Flywheel for Frequency Grid Support

Florian Reißner and Giovanni De Carne, *Senior Member, IEEE*

***Abstract*—With increasing penetration of inverter-connected power sources, such as renewable energy sources (RESs), the equivalent inertia in the grid decreases. Employing maximum power point tracking controllers, RESs behave like constant power sources, not offering damping to support the frequency during disturbances. Novel control algorithms have been proposed that can mimic the inertial behavior of generators or can provide grid support to counter the decline in system inertia. In this letter, we explore the capability of a *commercially* available high-speed flywheel energy storage system (FESS) to provide virtual inertia and damping services to microgrids. We demonstrate how a virtual synchronous machine algorithm can increase the grid inertia by controlling the FESS active power. A power hardware in the loop evaluation was performed considering the real limitations of a commercial flywheel with different virtual inertia and damping droop settings.**

***Index Terms*—Commercial flywheel, damping, energy storage, grid support, inertia, virtual synchronous machine (VSM).**

I. Introduction

MOTIVATED by the energy transition and the ensuing rise in inverter-interfaced power generation in the grid, control algorithms for inverters integrating *grid forming* (GFM) features have become an important area of research [1], [2], [3]. GFM inverters implement frequency and voltage support features, such as droop and virtual inertia. It has been shown that such inverters can form stable *microgrid*s (MGs) [4] and improve the system stability [5]. Numerous approaches exist to implement frequency support measures in inverter-interfaced power stations. While it is possible to implement grid support features also on *phase locked loop* (PLL)-controlled inverters (often referred to as *fast frequency support*), cf., [6], controllers emulating synchronous machines do not require a PLL at all and, therefore, offer superior stability and robustness in grids with high penetration of inverter-interfaced power sources. Reissner and Weiss [7] showed that *virtual synchronous machine* (VSM)-based inverters can also improve the region of attraction of a stable operating point of a grid.

Virtual inertia and active damping services can be provided only if energy is available on demand. Various ideas have been proposed to exploit existing energy reservoirs to provide grid support, such as the rotational energy of wind turbines [8] or the module capacitor energy in modular multilevel converters [9]. However, such approaches may only have very limited impact, since the available energy storage is often small. To overcome this, dedicated power reservoirs, such as super capacitors, batteries, or flywheels can be used [10], [11], [12], [13]. Theoretically, such energy storage provides instantly available power, only limited by the power rating of the relevant equipment and potential manufacturer constraints.

In this letter, we investigate the provision of active damping and virtual inertia services by a commercially available 120-kW high-speed *flywheel energy storage system* (FESS) in MGs, implemented using a VSM controller. We investigate the technological limitations of the FESS, such as the maximal power ramp rate, on offering frequency support in small MGs. Particular focus was placed on the potential overshoots and oscillations created by poor tuning. All necessary auxiliaries of commercially available FESS (vacuum pumps, air conditioning, etc.) have been included in the analysis in order to give a realistic estimate of the system performance.

The VSM and the MG were implemented on an Opal-RT 5700 real-time simulator, integrated with a 1-MVA *power hardware in the loop* (PHIL) test field in the Energy Lab 2.0 at the Karlsruhe Institute of Technology. The rest of this letter is organized as follows. In Section II, we briefly describe the VSM and the grid model used in the experiments. In Section III, we present the experimental results. Finally, Section IV concludes this letter.

II. System Description

Virtual Synchronous Machine: The VSM used in this letter is based on [14] and [15]. We show a simplified block diagram in Fig. 1 containing the active and reactive power control loops.

Manuscript received 24 January 2024; revised 13 February 2024; accepted 22 February 2024. Date of publication 26 February 2024; date of current version 4 September 2024. The work of Florian Reißner was supported in part by Israel Science Foundation under Grant 2802/21. The work of Giovanni De Carne was supported in part by the Helmholtz Association through the program "Energy System Design," and in part by the Helmholtz Young Investigator Group "Hybrid Networks" under Grant VH-NG-1613. *(Corresponding author: Florian Reißner.)*

Florian Reißner is with the School of Electrical Engineering, Tel Aviv University, Ramat Aviv 69978, Israel (e-mail: reissner@tauex.tau.ac.il).

Giovanni De Carne is with the Institute for Technical Physics, Karlsruhe Institute of Technology, 76344 Karlsruhe, Germany (e-mail: giovanni.carne@kit.edu).

Color versions of one or more figures in this article are available at https://doi.org/10.1109/TPEL.2024.3369980.

Digital Object Identifier 10.1109/TPEL.2024.3369980

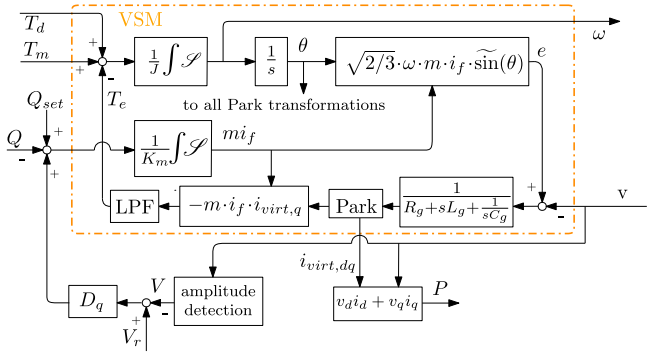

Fig. 1. Block diagram of the VSM with the main control loops for frequency, voltage, and reactive power, and a virtual impedance block.

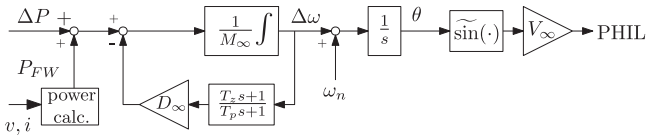

Fig. 2. Block diagram of the grid model (cf., [17, Sec. 11.1]).

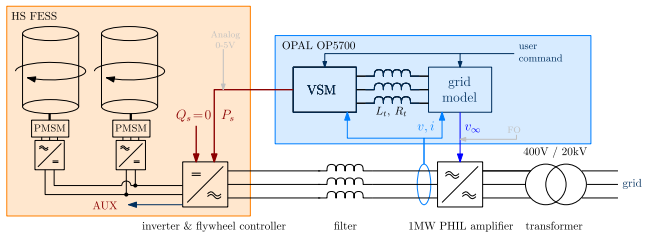

Fig. 3. FESS PHIL test field consisting of two Stornetic high-speed flywheels, interfaced with two 200-kVA Egston power amplifiers. An Opal-RT 5700 simulator executes both the VSM and the MG model.

The main part of the VSM consists of a second-order swing equation, expressed as a torque balance

$$J\omega = \int \mathscr{S}(T_m + T_d - T_e)\mathrm{d}t \tag{1}$$

where T_m, T_d, and T_e are the mechanical-, damping-, and electrical torque, respectively, J is the inertia constant, and ω is the angular frequency of the rotor of the VSM.[1] $\int \mathscr{S}$ denotes a saturating integrator (cf., [14]). In the following, we will also refer to the inertia using $M = J\omega_n$, where ω_n is the nominal grid frequency. The damping torque T_d is obtained from the following equation, expressed in the Laplace domain:

$$T_d(s) = \frac{D_l + D_h \tau s}{\tau s + 1}(\omega_n - \omega(s)) + T_w(s) \tag{2}$$

where τ is the time constant of the lead–lag filter, and D_l and D_h are the low- and high-frequency damping constants, respectively. When controlling a flywheel, the low-frequency droop constant D_l is set to zero, to not deplete the flywheel energy during long frequency deviations. We refer to the damping ratio of the VSM as $\rho = D_h/J$ in the following. $T_w(s)$ in (2) denotes the damper winding torque, as defined in [16], which we do not explain here for brevity. It essentially prevents oscillations of the VSM rotor, but has a little impact on the output power. Integrating ω (modulo 2π), the rotor angle θ is obtained, which then is used for all required Park-transformations. The virtual rotor field current i_f is obtained from the following equation, which implements voltage droop and reactive power control:

$$mi_f = \frac{1}{K_m} \int \mathscr{S}(D_q(V_r - V) + Q_{\text{set}} - Q)\mathrm{d}t \tag{3}$$

where $m > 0$ is the mutual inductance (a constant), $K_m > 0$ is the controller gain, D_q is the voltage droop factor, V_r and Q_{set} are the voltage and reactive power references, respectively, and V and Q are the measured voltage and reactive power. The synchronous internal voltages e are obtained from the following equation:

$$e = \sqrt{\frac{2}{3}} mi_f [\sin\theta \quad \sin(\theta - \tfrac{2}{3}\pi) \quad \sin(\theta + \tfrac{2}{3}\pi)]^\top. \tag{4}$$

[1]Note that the flywheel rotates at a much higher frequency (> 300 Hz).

Using a virtual impedance with resistance R_g, inductance L_g, and capacitance C_g, the virtual currents i_{virt} are obtained from $e - v$. This allows to calculate $\bar{T}_e = -mi_f i_{\text{virt},q}$, which after low-pass filtering by block low-pass filter (LPF) gives T_e.

MG model: The MG is represented by an infinite bus with frequency dynamics similar to those of a synchronous generator, cf., [17, Sec. 11.1]. The voltage amplitude V_∞ is assumed constant, and the equivalent inertia and droop constants are denoted by M_∞ and D_∞, respectively. The governor and turbine characteristics of this equivalent generator are represented by a first-order lead–lag filter with time constants T_z and T_p. A loss of a generation unit is simulated by a drop in the power production by ΔP, which subsequently causes a typical frequency drop with a *rate of change of frequency* (ROCOF) defined by the equivalent inertia M_∞ and a steady-state frequency deviation dictated by D_∞. T_z and T_p are chosen such that the nadir is about three times the steady-state deviation and occurs approximately after 6 s. The output power of the flywheel P_{FW} is calculated from voltage and current measurements and added to ΔP. The block representation of this grid model is shown in Fig. 2.

III. Experimental Results

The experimental setup is shown in Fig. 3. A Stornetic high-speed FESS is used as an energy storage system with a maximum capacity of 7.2 kWh (cf., Fig. 4). The FESS consists of two high-speed 60-kW flywheels. Several auxiliaries of the FESS, such as the temperature unit, a vacuum pump, and a control equipment add an average consumption of 2–6 kW, according to ambient temperature and operating point [18]. The dynamics of the inner control loops of the FESS are assumed to be negligible for the present analysis. The test grid is powered by two 200-kVA Compiso Egston power amplifiers, connected with an Opal-RT 5700 real-time simulator through fiber optics. The simulated MG shown in Section II is connected to a VSM through a line impedance of $L_t = 0.1$ mH and $R_t = 0.1\Omega$. The VSM sends a power reference in the range of $P_s \in [-120\,120]$ kW to the FESS which, in order to ensure low latency, is encoded as an

Fig. 4. Photograph of the Stornetic FESS with the two 60-kW flywheels.

analog voltage between 0 and 5 V. The ramp rate r of this power setpoint P_s is configurable, with a maximum value of ± 80 kW/s, limited by manufacturer safeguards. The reactive power setpoint is $Q_s \equiv 0$ kVAr. In total, three probes measure the voltages v and currents i at the terminals of the PHIL amplifier, which then are used to estimate the output power P_{FW} of the flywheel. In our tests, we simulate the loss of a generation unit in the MG by imposing a step change of $\Delta P = -80$ kW on the grid model in Fig. 2 and observe the frequency dynamics of the system. We then investigate the influence of the ramp rate r, the VSM parameters inertia $M = J\omega_n$, the high frequency droop expressed as $\rho = D_h/J$, and droop time constant τ on the nadir, ROCOF, and the amplitude of the occurring oscillations. The MG is assumed to have a nominal power of 1 MW with an inertia constant of $M_\infty = 23.9\text{kWs}^2$ which, expressed in seconds, corresponds to $H_\infty = 3.75$ s. The droop constant is 5%, i.e., $D_\infty = 63.7$ kWs and the nominal grid voltage is $V_\infty = 230$ Vrms. $T_p = 15$ s and $T_z = 3$ s are chosen similar to values in [4]. The tuning parameters of the VSM are chosen such that for a frequency drop with a nadir of 49 Hz (the minimum tolerated frequency of the FESS), the VSM produces approximately the maximum power output of 120 kW. For the VSM, we use $\tau \in \{0, 0.5, 2\}$, $\rho \in \{0, 1, 2\}$, and $M \in \{31.8, 47.7\}\text{kWs}^2$, and all other parameters are tuned according to [15]. The ramp rates tested are $r \in \{40, 80\}$ kW/s. In the following, we show plots of frequency and power for selected experiments, before analyzing the influence of the tuning parameters on the grid behavior.

A. Frequency and Power Response

Figs. 5 and 6 show the influence of the time constant τ of the high-pass filter and the ramp rate r on the frequency of the system and the output power of the FESS. Clearly, a higher τ (meaning a slower washout time of the high-pass filter) improved the nadir and decreased the initial oscillation caused by the ramp rate limitation. (Note that $\tau = 0$ means no frequency droop.) The ramp rate had no significant impact on the nadir, but a slower ramp rate causes more initial overshoot. For better readability, we omitted plotting the power output for $\tau = 0.5$ s in Fig. 6, instead we plot both the measured output power P_{FW} (solid lines)

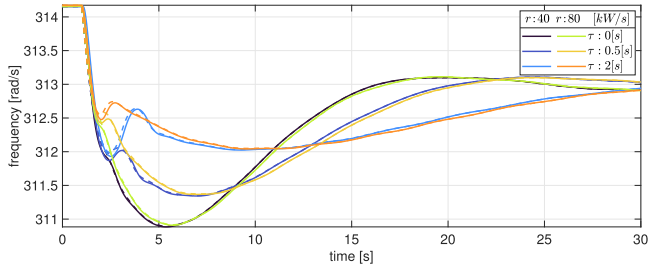

Fig. 5. Frequency of the grid (dashed line) and the VSM (solid line) subsequent to a ΔP step of 80 kW. Higher τ decreases the nadir, and a lower r causes higher oscillations. $\rho = 2\text{s}^{-1}$ and $M = 31.8\text{kWs}^2$.

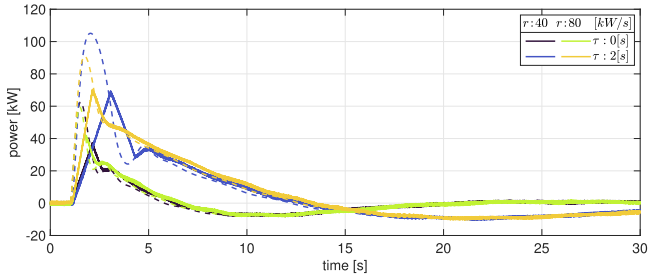

Fig. 6. Output power of the FESS (solid line) and the VSM (dashed line) subsequent to a loss of a 80-kW power unit. The impact of the rate limitation r is clearly visible. $\rho = 2\text{s}^{-1}$ and $M = 31.8\text{kWs}^2$.

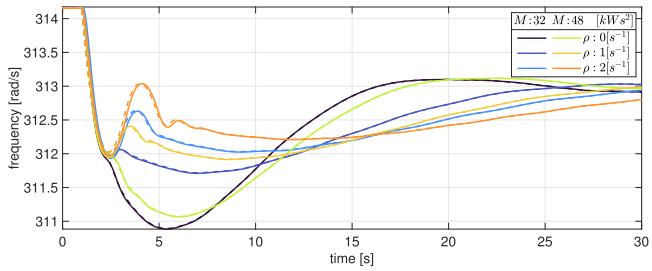

Fig. 7. Frequency response of the grid (solid line) and the VSM (dashed line) for a variation of M and ρ. $\tau = 2$s and $r = 40\,\text{kW/s}$.

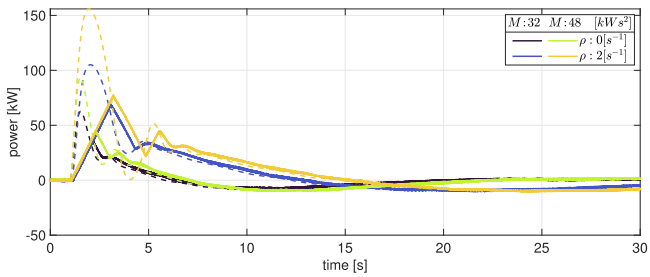

Fig. 8. FESS output power (solid line) initially cannot follow P_s (dashed line) due to the ramp limitation. $\tau = 2$s and $r = 40\,\text{kW/s}$.

and the reference power P_s (dashed lines). Clearly, the effect of the ramp limitation can be seen in the time interval between 0 and 5 s.

Figs. 7 and 8 show a comparison of the frequency and power response for a variation of M and ρ. Clearly, increasing either parameter improves the frequency nadir, while the initial ROCOF and the initial oscillation (with a minimum of 312 rad/s) remain

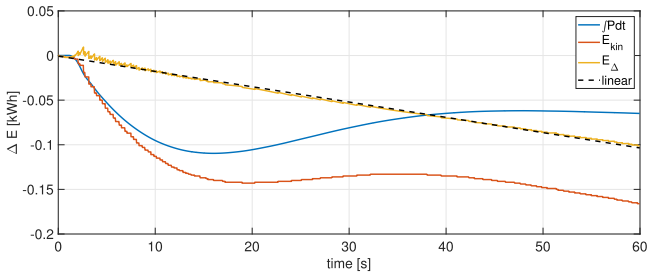

Fig. 9. Relative depletion of the flywheel during one experiment.

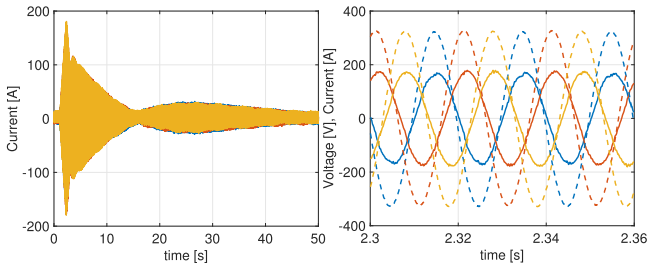

Fig. 10. Current at the terminals of the FESS during an experiment (left-hand side) and a zoomed in section at the peak including the voltages (dashed lines) on the right-hand side.

unchanged. This can be understood from Fig. 8, where the ramp rate limitation on P_s forces identical P_{FW} for all parameters, up to approximately 2 s. In consequence, the inertia initially cannot slow down the frequency decline such that the slope of the frequency is dictated by M_∞.

Fig. 9 shows the amount of energy extracted from the flywheels, ΔE_{kin} (red) and the integral of the power P_{FW} flowing to the MG for an experiment with $M = 47.7\,\text{kWs}^2$, $\rho = 2\text{s}^{-1}$, and $\tau = 2$s. The difference between the two (yellow) is the energy consumed by the auxiliaries of the flywheels. A first-order line fit (black dashed line) indicates that the auxiliaries consumed approx. 6 kW in this experiment. Due to the consumption of the auxiliaries, in a real scenario, P_s must account for these power losses. Fig. 10 shows the currents and voltages at the terminals of the amplifiers during this experiment. A peak of 180 A per line is reached.

B. Parameter Study

We show the impact of all four parameters r, ρ, τ, and M on nadir, ROCOF, and oscillations in the following analysis. Where applicable, solid lines are used for $r = 40$ kW/s and dashed lines for $r = 80$ kW/s. Recall that if $\rho = 0$, also $\tau = 0$, and vice versa. None of the parameters shows relevant impact on the ROCOF, cf., Fig. 11(a). This is due to the RoCoF being maximal at the onset of the disturbance, while due to the finite response time of the flywheel, P_{FW} starts to impact the system only after approx. 0.5 s. Clearly, A^{osc} tends to zero for increasing r, cf., Fig. 11(b). Indeed, for most tunings, A^{osc} is already negligible at 80 kW/s, such that r is not required to be much faster. While higher M, ρ, and τ all increase A^{osc}, a higher r decreases oscillations, cf., Fig. 12(a). Finally, the nadir improves with τ, ρ, and M, see Fig. 12(b), suggesting that both HF-droop and

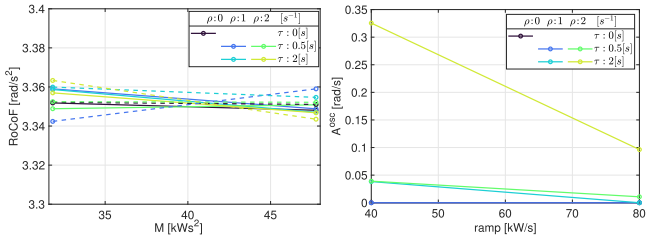

Fig. 11. Impact of r, τ, and ρ on ROCOF (l) and oscillations (r). $A^{\text{osc}} = 0$ for $\rho = 0\text{s}^{-1}$, such that the black curve is hidden.

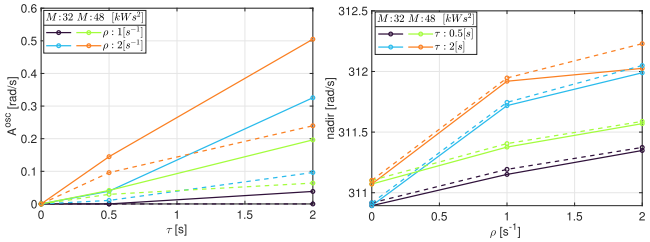

Fig. 12. Impact of ρ, τ, and M on oscillations (l) and nadir (r).

inertia can improve system performance, giving the designer relative freedom to tune these parameters to exploit a maximum amount of energy from the FESS according to the application.

IV. Conclusion

This letter shows the performance of a commercially available high-speed FESS controlled by a VSM to provide frequency support to an MG. The flywheel used in these experiments has a nominal power of 120 kW and is able to emulate an inertia of $47.7\,\text{kWs}^2$, which is comparable with the one of a 1-MW synchronous generator. The power setpoint was rate-limited by the flywheel, which causes damped oscillations in the first few seconds subsequent to a simulated loss in power generation in the MG. The ROCOF in such a scenario can only be impacted marginally, if such a ramp limitation is too aggressive. For higher ramp rates and adequate tuning, only little oscillations occur and the frequency nadir can be improved significantly by the FESS. Further work is planned to combine the FESS with a supercapacitor to compensate for the ramp rate limitation and to test both in a realistic MG.

References

[1] F. Mandrile, E. Carpaneto, and R. Bojoi, "Grid-feeding inverter with simplified virtual synchronous compensator providing grid services and grid support," *IEEE Trans. Ind. Appl.*, vol. 57, no. 1, pp. 559–569, Jan./Feb. 2021.

[2] V. Mallemaci, F. Mandrile, S. Rubino, A. Mazza, E. Carpaneto, and R. Bojoi, "A comprehensive comparison of virtual synchronous generators with focus on virtual inertia and frequency regulation," *Electric Power Syst. Res.*, vol. 201, 2021, Art. no. 107516.

[3] R. Rosso, X. Wang, M. Liserre, X. Lu, and S. Engelken, "Grid-forming converters: Control approaches, grid-synchronization, and future trends–a review," *IEEE Open J. Ind. Appl.*, vol. 2, pp. 93–109, 2021.

[4] F. Reissner, V. Mallemaci, F. Mandrile, R. Bojoi, and G. Weiss, "Virtual friction subjected to communication delays in a microgrid of virtual synchronous machines," *IEEE J. Emerg. Sel. Topics Power Electron.*, vol. 11, no. 4, pp. 3910–3923, Aug. 2023.

[5] B. K. Poolla, D. Groß, and F. Dörfler, "Placement and implementation of grid-forming and grid-following virtual inertia and fast frequency response," *IEEE Trans. Pow. Sys.*, vol. 34, no. 4, pp. 3035–3046, Jul. 2019.

[6] X. Zhao, Y. Xue, and X.-P. Zhang, "Fast frequency support from wind turbine systems by arresting frequency nadir close to settling frequency," *IEEE Open Access J. Power Energy*, vol. 7, pp. 191–202, 2020.

[7] F. Reissner and G. Weiss, "The region of attraction of a grid with virtual synchronous machines employing virtual friction," in *Proc. 13th IEEE Int. Symp. Power Electron. Distrib. Gener. Syst.*, 2022, pp. 1–6.

[8] J. Morren, J. Pierik, and S. W. De Haan, "Inertial response of variable speed wind turbines," *Electric Power Syst. Res.*, vol. 76, no. 11, pp. 980–987, 2006.

[9] D. Wiemann, T. Hassan, and S. Dieckerhoff, "Grid-forming control of an MMC STATCOM using submodule capacitors to emulate inertia," in *Proc. IEEE 14th Int. Symp. Power Electron. Distrib. Gener. Syst.*, 2023, pp. 854–861.

[10] J. A. Suul, S. D'Arco, and G. Guidi, "Virtual synchronous machine-based control of a single-phase bi-directional battery charger for providing vehicle-to-grid services," *IEEE Trans. Ind. Appl.*, vol. 52, no. 4, pp. 3234–3244, Jul./Aug. 2016.

[11] S. Karrari, G. De Carne, and M. Noe, "Adaptive droop control strategy for flywheel energy storage systems: A power hardware-in-the-loop validation," *Electric Power Syst. Res.*, vol. 212, 2022, Art. no. 108300.

[12] S. Karrari, H. R. Baghaee, G. D. Carne, M. Noe, and J. Geisbuesch, "Adaptive inertia emulation control for high-speed flywheel energy storage systems," *IET Gener., Transmiss. Distrib.*, vol. 14, no. 22, pp. 5047–5059, 2020.

[13] H. Kikusato et al., "Flywheel energy storage system based microgrid controller design and PHIL testing," *Energy Rep.*, vol. 8, pp. 470–475, 2022.

[14] Z. Kustanovich, F. Reissner, S. Shivratri, and G. Weiss, "The sensitivity of grid-connected synchronverters with respect to measurement errors," *IEEE Access*, vol. 9, pp. 118985–118995, 2021.

[15] Z. Kustanovich, S. Shivratri, H. Yin, F. Reissner, and G. Weiss, "Synchronverters with fast current loops," *IEEE Trans. Ind. Electron.*, vol. 70, no. 11, pp. 11357–11367, Nov. 2023.

[16] H. Yin, Z. Kustanovich, and G. Weiss, "Attenuation of power system oscillations by using virtual damper windings," in *Proc. IEEE 23rd Workshop Control Model. Power Elec.*, 2022, pp. 1–6.

[17] P. Kundur, N. J. Balu, and M. G. Lauby, *Power System Stability and Control*, vol. 7. New York, NY, USA: McGraw-hill, 1994.

[18] S. Karrari, G. De Carne, and M. Noe, "Model validation of a high-speed flywheel energy storage system using power hardware-in-the-loop testing," *J. Energy Storage*, vol. 43, 2021, Art. no. 103177.